Olfactory sensory neurons mediate ultrarapid antiviral immune responses in a TrkA-dependent manner

Ali Sepahi[a], Aurora Kraus[a], Elisa Casadei[a], Christopher A. Johnston[b], Jorge Galindo-Villegas[c,d], Cecelia Kelly[a], Diana García-Moreno[c], Pilar Muñoz[e], Victoriano Mulero[c], Mar Huertas[f], and Irene Salinas[a,1]

[a]Center of Evolutionary and Theoretical Immunology, Biology Department, University of New Mexico, Albuquerque, NM 87131; [b]Biology Department, University of New Mexico, Albuquerque, NM 87131; [c]Department of Cell Biology and Histology, Faculty of Biology, Instituto Murciano de Investigación Biosanitaria-Arrixaca, Campus Universitario de Espinardo, University of Murcia, 30100 Murcia, Spain; [d]Faculty of Biosciences and Aquaculture, Nord University, 8049 Bodø, Norway; [e]Department of Faculty of Veterinary, University of Murcia, 30100 Murcia, Spain; and [f]Department of Biology, Texas State University, San Marcos, TX 78666

Edited by Lalita Ramakrishnan, University of Cambridge, Cambridge, United Kingdom, and approved May 10, 2019 (received for review January 5, 2019)

The nervous system regulates host immunity in complex ways. Vertebrate olfactory sensory neurons (OSNs) are located in direct contact with pathogens; however, OSNs' ability to detect danger and initiate immune responses is unclear. We report that nasal delivery of rhabdoviruses induces apoptosis in crypt OSNs via the interaction of the OSN TrkA receptor with the viral glycoprotein in teleost fish. This signal results in electrical activation of neurons and very rapid proinflammatory responses in the olfactory organ (OO), but dampened inflammation in the olfactory bulb (OB). CD8α$^+$ cells infiltrate the OO within minutes of nasal viral delivery, and TrkA blocking, but not caspase-3 blocking, abrogates this response. Infiltrating CD8α$^+$ cells were TCRαβ T cells with a nonconventional phenotype that originated from the microvasculature surrounding the OB and not the periphery. Nasal delivery of viral glycoprotein (G protein) recapitulated the immune responses observed with the whole virus, and antibody blocking of viral G protein abrogated these responses. Ablation of crypt neurons in zebrafish resulted in increased susceptibility to rhabdoviruses. These results indicate a function for OSNs as a first layer of pathogen detection in vertebrates and as orchestrators of nasal–CNS antiviral immune responses.

neuroimmunology | olfactory sensory neurons | teleost | viral immunity | TrkA

The interactions between the nervous system and the immune system are multiple and complex. Both systems are specialized in sensing and responding to environmental signals, and, evolutionarily speaking, these two systems may have originated from a common ancestral precursor cell type (1). Sensory neurons have been shown to participate in immune responses in several organisms. For instance, in mice, nociceptor sensory neurons can be directly activated by bacteria to control pain and modulate inflammatory responses (2, 3). Moreover, sensory neurons are critical for suppressing innate immune responses triggered by pathogens and restore host homeostasis in invertebrates (4).

Vertebrate olfactory sensory neurons (OSNs) rapidly sense chemical stimuli present in the environment and transduce odorant-encoded signals into electrical signals that travel to the olfactory bulb (OB), via the olfactory nerve, where they are integrated and transferred to other parts of the central nervous system (CNS). OSNs are one of the few neurons in the vertebrate body that are in direct contact with the external environment, yet the interactions between microbes and OSNs remain unknown. OSNs are also in close proximity to a local network of immune cells known as the nasopharynx-associated lymphoid tissue (NALT), which is present in both teleosts and mammals (5, 6). The cross-talk between OSNs and NALT during the course of an immune response has not yet been investigated.

Crypt neurons are a type of OSN present in fish with enigmatic function although recent evidence suggests that these neurons are responsible for kin recognition in zebrafish (7). Crypt neurons only express one type of olfactory receptor, the vomeronasal receptor 1-like Ora4 and can be identified by their tropomyosin-related kinase A receptor (TrkA) immunoreactivity (8–10). The interaction between TrkA and endogenous ligands, such as nerve growth factor (NGF), induces internalization of TrkA into endosomes (11). While TrkA activation by NGF regulates neuronal differentiation, growth, and survival (12, 13), previous studies have shown the ability of pathogens to hijack the TrkA system to infect hosts (14).

Many neurotropic viruses exploit the olfactory route to infect CNS tissues (15, 16). In this study, using infectious hematopoietic necrosis virus (IHNV), an aquatic rhabdovirus with neurotropic characteristics (17), we report that crypt neurons expressing TrkA are fast sensors of viruses in the olfactory mucosa and critical regulators of antiviral immune responses in teleost fish. Our results reveal mechanisms of neuroimmune cooperation against viruses in the nasal mucosa and the CNS of vertebrates.

Results

Nasal Delivery of Neurotropic Virus Induces Caspase-3–Dependent Apoptosis in TrkA$^+$ Crypt Neurons. Neurotropic viruses such as rhabdoviruses can infect OSNs and transneuronally infect the CNS (15, 16). Viruses can also cause caspase-dependent apoptosis in neurons via NGF signals (18–21). We first confirmed that anti-TrkA antibody primarily labels crypt neurons in rainbow trout

Significance

Many pathogens exploit the olfactory route to gain entry into the host. Olfactory sensory neurons (OSNs) are responsible for the detection of chemical stimuli in the environment but are also continuously exposed to microorganisms. Here, we report the interaction between crypt neurons (unique OSNs present in fish) and fish rhabdoviruses, an interaction that led to fast immune responses and the recruitment of nonconventional CD8 T cells to the olfactory mucosa from the olfactory bulb. These previously unrecognized antiviral immune responses required neuronal activation and depended on the interaction between the TrkA receptor expressed by crypt neurons and the viral glycoprotein protein. Our results show the importance of sensory neurons in sensing and controlling viruses that invade the nasal mucosa.

Author contributions: A.S., A.K., J.G.-V., V.M., and I.S. designed research; A.S., A.K., E.C., C.A.J., C.K., D.G.-M., P.M., M.H., and I.S. performed research; C.A.J., D.G.-M., and V.M. contributed new reagents/analytic tools; A.S., A.K., E.C., J.G.-V., P.M., V.M., M.H., and I.S. analyzed data; and A.S., A.K., V.M., M.H., and I.S. wrote the paper.

The authors declare no conflict of interest.

This article is a PNAS Direct Submission.

[1]To whom correspondence may be addressed. Email: isalinas@unm.edu.

This article contains supporting information online at www.pnas.org/lookup/suppl/doi:10.1073/pnas.1900083116/-/DCSupplemental.

Published online June 3, 2019.

(*Oncorhynchus mykiss*). As previously reported, TrkA$^+$ cells in the olfactory organ (OO) of trout had typical morphology and apical localization of crypt cells (Fig. 1*A*). Immunoblotting of total tissue lysates with rabbit anti-TrkA antibody showed a band at the expected size of ∼130 kDa in OO, but not in the head-kidney (HK), the main hematopoietic tissue in bony fish or the OB (*SI Appendix*, Fig. S1*A*). Microscopy results confirmed the absence of TrkA$^+$ cells in HK (*SI Appendix*, Fig. S1*B*), indicating that trout immune cells are not TrkA$^+$, at least by IF microscopy. When we delivered IHNV intranasally (IN) into rainbow trout, we observed a significant decrease in the number of TrkA$^+$ crypt cells in the OO, compared with control fish, 15 min, 1 h, and 1 d after treatment (Fig. 1 *A*, *B*, *E*, and *M*). The number of TrkA$^+$ crypt cells returned to basal levels by day 4, suggesting that replacement from progenitors takes ∼4 d to complete (Fig. 1*M*). Loss of TrkA reactivity 15 min after viral delivery suggested internalization of the TrkA receptor and was associated with the presence of apoptotic-like morphology in the remaining TrkA$^+$ crypt cells (Fig. 1 *B*, *D*, *H*, *J*, *K*, and *M*), compared with controls (Fig. 1 *A*, *C*, *G*, *I*, *K*, and *M*). TrkA signaling may result in cell death in sensory neurons (22). In agreement, staining with anti–caspase-3 antibody that labels cleaved caspase-3 confirmed that trout crypt neurons were undergoing apoptosis 15 min after nasal viral delivery (Fig. 1 *E* and *F*), as did positive controls that had received poly I:C intranasally (*SI Appendix*, Fig. S2*A*). Pharmacological blockade of TrkA with the drug AG879 (Fig. 1*L*) rescued 50% of TrkA reactivity in crypt neurons (Fig. 1*N*) and also abolished IHNV-induced caspase-3 apoptosis (*SI Appendix*, Fig. S2*C*). Combined,

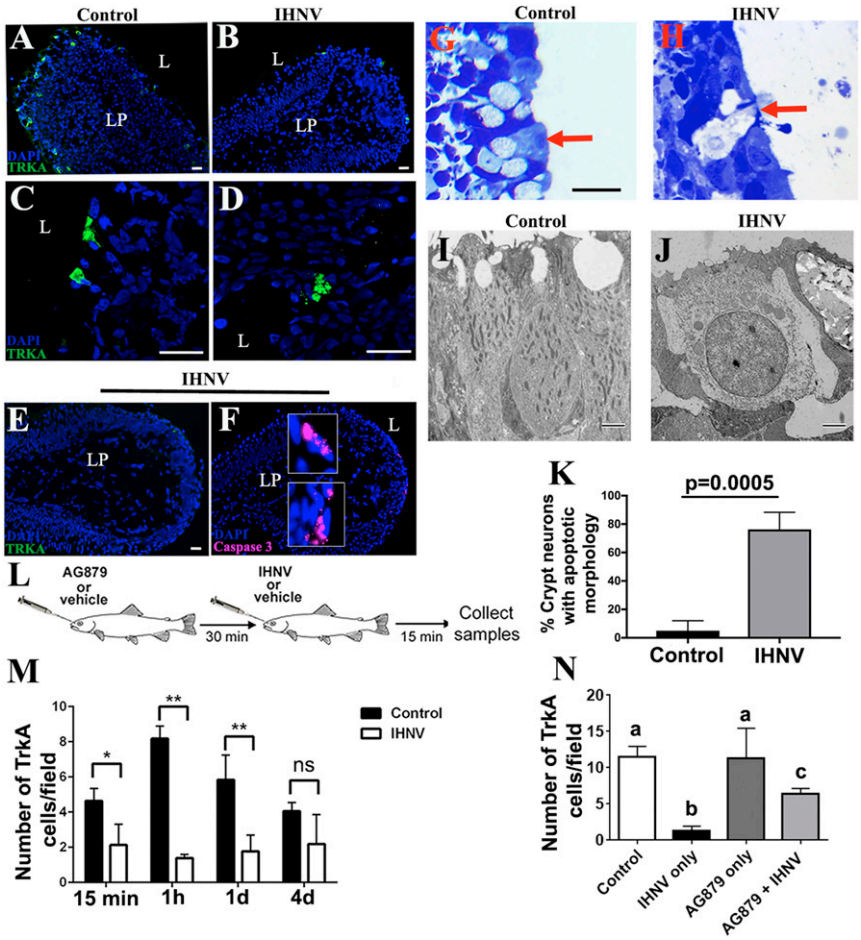

Fig. 1. Nasal delivery of neurotropic virus induces caspase-3–dependent apoptosis to TrkA$^+$ crypt neurons. IF microscopy image of rainbow trout OO cryosections (*A*) Control and (*B*) 15 min after nasal IHNV delivery stained with anti-TrkA (FITC, green) show a decrease in the number of TrkA$^+$ crypt neurons following IN delivery of IHNV. Nuclei were stained with nuclear stain DAPI (blue). Confocal microscopy images of rainbow trout OO cryosections (*C*) Control and (*D*) 15 min after nasal IHNV delivery stained with anti-TrkA (FITC, green) showing changes in TrkA reactivity with the characteristic morphology of cell apoptosis in TrkA$^+$ cells following IN delivery of IHNV. (Scale bars: 20 μm.) IF staining of an IHNV-vaccinated rainbow trout OO 15 min after IN delivery with anti-TrkA (FITC, green) (*E*) and anti–caspase-3 (Cy5, magenta) (*F*) showing colocalization of caspase-3 staining in low-TrkA$^+$ crypt neurons. (Scale bars: 20 μm.) Cell nuclei were stained with DAPI DNA stain (blue). Results are representative of three independent experiments ($n = 5$). L, lumen; LP, lamina propria. Semithin sections of control (*G*) and IHNV-treated (*H*) rainbow trout OO ($n = 3$) indicate that crypt neurons undergo cell death following viral delivery. (Scale bars: *A*–*H*, 20 μm.) Transmission electron microscopy (TEM) showing a crypt neuron in control trout OO (*I*) and a crypt neuron undergoing cell death in IHNV-treated OO (*J*) ($n = 3$). (Scale bars: 2 μm.) (*K*) Quantification of crypt neurons with apoptotic morphology. Crypt neurons were counted ($n = 10$ to 20) from semithin sections and morphology scored as healthy or apoptotic/dead. Data are shown as the percentage of crypt neurons with apoptotic morphology. $n = 3$ fish per treatment. (*L*) Schematic diagram of the experimental design used in the TrkA-blocking experiment. AG879 or vehicle was delivered IN, and, 30 min later, IHNV or PBS (control) was delivered to the nasal cavity. OO and OB were collected 15 min after IHNV delivery. (*M*) Quantification of the mean number of TrkA$^+$ crypt neurons in control and nasal IHNV-treated rainbow trout OO 15 min, 1 h, 1 d, and 4 d after nasal viral delivery, showing that TrkA reactivity begins to recover on day 4 ($n = 3$). Results are expressed as mean ± SEM. Unpaired *t* test, $*P < 0.05$, $**P < 0.01$. ns, not significant. (*N*) AG879 pretreatment partially abolishes loss of IHNV-induced TrkA reactivity in crypt neurons ($n = 3$). Results are expressed as mean ± SEM. Different letters indicate statistically different groups using one-way ANOVA and Tukey post hoc analysis test. $P < 0.05$.

these results indicate that aquatic rhabdoviruses result in TrkA internalization and downstream cell death in rainbow trout crypt neurons.

Rainbow Trout Smell Neurotropic Virus. Exposure of either live attenuated IHNV or culture medium used to grow the virus elicited strong olfactory responses and followed a dose-dependent pattern characteristic of activation of olfactory receptors (Fig. 2*A*). Consequently, when we exposed the OO to higher concentration of stimuli, we recorded higher normalized olfactory responses, which mean an increased number of activated olfactory receptors. Both the virus and the culture medium elicited highly sensitive olfactory responses, which could be detected up to a $1{:}10^5$ dilution by electroolfactogram (EOG). However, IHNV elicited significantly greater olfactory responses than culture medium at the 1:100 dilution (paired *t* test, $P < 0.05$). Differences in the slopes of the linear dose–responses also suggested activation of a different receptor set for each stimulus. Thus, we performed cross-adaptation experiments, in which the OO was continuously saturated with IHNV (adapted stimulus), and then measured olfactory responses to IHNV (self-adapted control) or a mix of IHNV with medium by EOG (*SI Appendix*). We repeated the same experiment, saturating the OO with medium and then measuring responses to medium alone or the IHNV and medium mix. If IHNV and medium activate different receptors, we would expect that OO saturated with IHNV will have a smaller olfactory response to a concentrated solution of IHNV, due to fewer IHNV receptors available for activation. In turn, we would expect a greater response for the mix of IHNV and medium since medium-specific receptors, but no IHNV-specific receptors, would be available for activation. In agreement, cross-adaptation odorant assays showed that, after saturation of olfactory receptors with the adapting solution, normalized self-adapted controls had significantly lower responses (26 to 40%, paired *t* test $P < 0.05$) than the mixture of IHNV and culture medium (Fig. 2*B*), which implied different activation of receptors by the virus and medium, respectively.

Since we hypothesized that viral detection is TrkA receptor-mediated, we expected a decrease of olfactory responses after nasal exposure to TrkA inhibitor AG879. Inhibition curves showed that AG879 affected the olfactory responses to virus and culture medium in concentrations of the drug as low as 10^{-8} M, with a total inhibition of activity at 10^{-5} M (Fig. 2 *C* and *D*). The inhibition of olfactory responses by the drug was significantly stronger (paired *t* test, $P < 0.05$) for the virus than the medium, with an inhibition of 50% of olfactory responses (EC_{50}) by AG879 of $10^{-6.3}$ M and 10^{-6} M for virus and medium, respectively. Inhibitory curves also suggested hormesis (biphasic dose–responses at different concentrations) at 10^{-7} M for the virus, but not for the medium; further studies are necessary to demonstrate a positive effect of the drug for virus detection at very low concentrations. Combined, these experiments demonstrate that the rainbow trout is able to smell viruses via TrkA signaling.

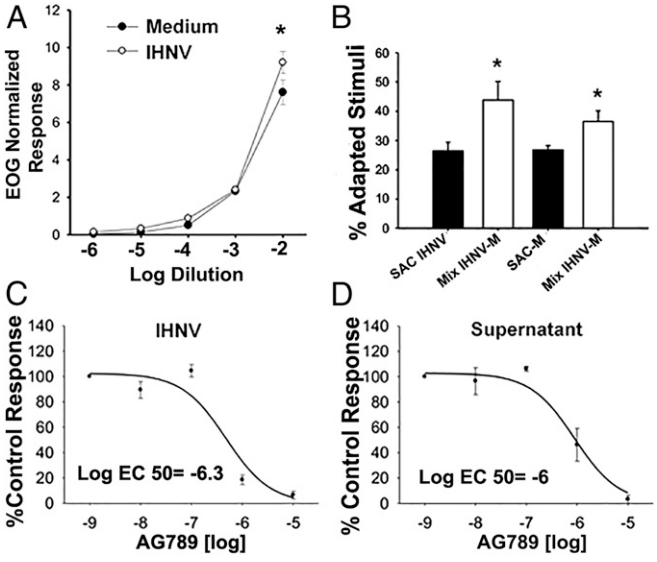

Fig. 2. Rainbow trout smell neurotropic virus. (*A*) Olfactory responses to IHNV and medium where the virus was grown (negative control) produce different dose–response curves in rainbow trout measured by electro-olfactogram (EOG). Responses were normalized to the L-Serine control. Data are represented as the mean ± SEM ($n = 8$ fish, two independent experiments). Paired *t* test showed significant differences (asterisk) at dilution 1:100 ($P < 0.05$). (*B*) IHNV activates a set of receptors different from those activated by virus-free medium (negative control). Cross-adaptation experiments compared olfactory responses to IHNV [self-adapted control (SAC)] or a mix of virus and the virus-free medium (Mix IHNV-M) when the OO was saturated with IHNV (adapted stimuli) odors. The same experiments were performed using the IHNV culture medium as adapted stimuli. Paired *t* test showed significant differences ($P < 0.05$) between both SAC and Mix ($n = 9$, one experiment). (*C*) AG879 treatment results in stronger inhibition of olfactory responses in IHNV than in virus-free supernatant ($n = 4$, one experiment). (*D*) Total pharmacological inhibition of olfactory responses was achieved at concentrations of the drug $>10^{-5}$ M. Paired *t* test showed significant differences ($P < 0.05$) between EC_{50} ($n = 9$, one experiment).

Neurotropic Viruses Activate Sensory Neurons in the OO and OB in a TrkA-Dependent Manner. Studies in fish have demonstrated that pERK staining and *c-fos* gene expression are suitable markers of neuronal activation upon odorant exposure in the OO and CNS (23, 24). However, whether viruses activate neurons in the OO and OB has not been investigated. Incubation of OO single cell suspensions with IHNV in vitro showed a significant increase in pERK labeling after 15 min, as measured with ∼3.5% of all cells being activated compared with controls (*SI Appendix*, Fig. S3 *A* and *B*). These results were confirmed in vivo by positive pERK staining in neurons of the OO and OB of IHNV-treated fish, but not controls (Fig. 3 *A–D* and *G*), as well as by the increased levels of total pERK in the OO and OB of IHNV-treated fish compared with controls shown by immunoblotting (*SI Appendix*, Fig. S3 *C* and *D*). OB neuronal activation was due to viral-derived signals present in the OO because IHNV was undetectable in the OB 15 min after nasal delivery (*SI Appendix*, Fig. S4 *A–E*). Interestingly, $pERK^+$ cells in the OO of IHNV-treated fish were localized in the middle of the neuroepithelium and did not have a crypt neuron morphology, indicating that OSNs other than crypt neurons become activated following nasal viral delivery (Fig. 3*C*). We also found a significant up-regulation in *c-fos* expression in the OO, but not the OB, in fish that received IHNV, compared with controls (Fig. 3*H*). Inhibition of the TrkA signaling pathway with AG879 before IN IHNV delivery blocked neuronal activation, as evidenced by the lack of pERK staining in the OO and OB and absence of *c-fos* up-regulation in the OO (Fig. 3 *E–H*). Combined, these data indicate that IHNV induces OSN activation through a TrkA-dependent pathway or, alternatively, that crypt neuron cell death results in activation of other OSNs.

Nasal Delivery of Viruses Results in Ultrarapid Innate Immune Responses in the OO and the CNS in a TrkA-Dependent Manner. We first performed histological examination of the OO and observed a trend toward enlarged lamina propria (LP) in IHNV-treated fish, compared with control fish, although it did not reach statistical significance (*SI Appendix*, Fig. S5). Histological changes in the OO were paralleled by changes in the expression of innate immune genes, including *ck10*, a CCL19-like chemokine in rainbow trout (25), and *ptgs2b* in OO 15 min after IHNV delivery. In the OB, in turn, we observed a significant down-regulation of *ck10* expression and no significant change in expression of *ptgs2b* (Fig. 4*A*). *ifng* expression was down-regulated both in the OO (twofold)

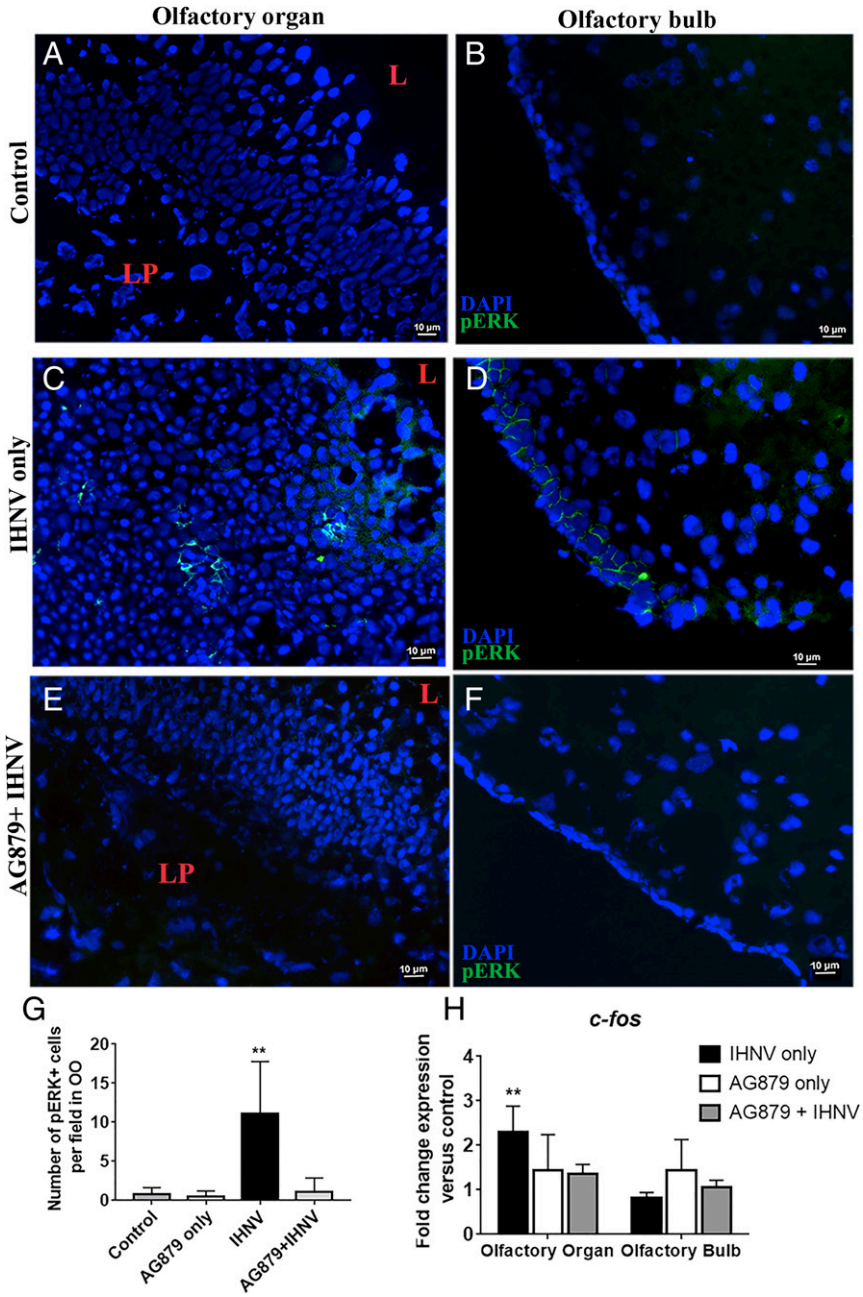

Fig. 3. Nasal IHNV delivery activates sensory neurons in the OO and OB in a TrkA-dependent manner. Shown is IF staining of control rainbow trout OO (*A*) and OB (*B*) cryosections stained with anti-pERK (FITC, green), showing absence of neuronal activation. Shown is IF staining of OO (*C*) and OB (*D*) cryosections of trout nasally treated with IHNV stained with anti-pERK antibody (FITC, green), showing neuronal activation 15 min after viral delivery. Shown is IF staining of rainbow trout OO (*E*) and OB (*F*) treated with AG879 + IHNV with anti-pERK, showing AG879 inhibition of viral-induced neuronal activation in both OO and OB. (Scale bars: 10 μm.) For *A*–*F*, cell nuclei were stained with DAPI DNA stain. (*G*) Quantification of pERK$^+$ cells in OO frozen sections from control, AG879 only, IHNV only, and AG879 + IHNV. Data are expressed as the mean number of pERK$^+$ cells per field (n = 3, 10 fields per fish). (*H*) Gene expression levels of *c-fos* in control, nasal IHNV-treated, AG879 only-treated and IHNV + AG879 groups as measured by RT-qPCR. Gene expression levels were normalized to elongation factor 1 alpha (*EF-1a*) and expressed as the fold-change compared with the control group, using the Pfaffl method. Results (*A*–*G*) are representative of three independent experiments (n = 5). Results were analyzed by unpaired t test, $^{**}P < 0.01$.

and the OB (fourfold) (Fig. 4*A*) whereas no significant changes in *tnfa* expression were recorded in any tissue or treatment. Importantly, when we pharmacologically blocked TrkA, we could revert IHNV-elicited changes in immune gene expression, such as *ck10* and *ptgs2b*, in both the OO and OB (Fig. 4*A*). In other cases, such as *ifng*, blocking of TrkA reverted the down-regulation of expression in the OB but had no significant change in the OO. No significant change in *tnfa* expression was observed between different treatments groups or tissues (Fig. 4*A*). These results indicate that antiviral proinflammatory immune responses in the nasal mucosa are accompanied by dampened antiviral immune responses in the OB and that these responses require TrkA activation in crypt neurons.

CD8α T Cells Rapidly Infiltrate the Olfactory Organ in a TrkA-Dependent Manner. Flow cytometry studies following IHNV IN delivery showed that the percentages of trout IgM$^+$, IgT$^+$ B cells, and CD8α$^+$ T cells

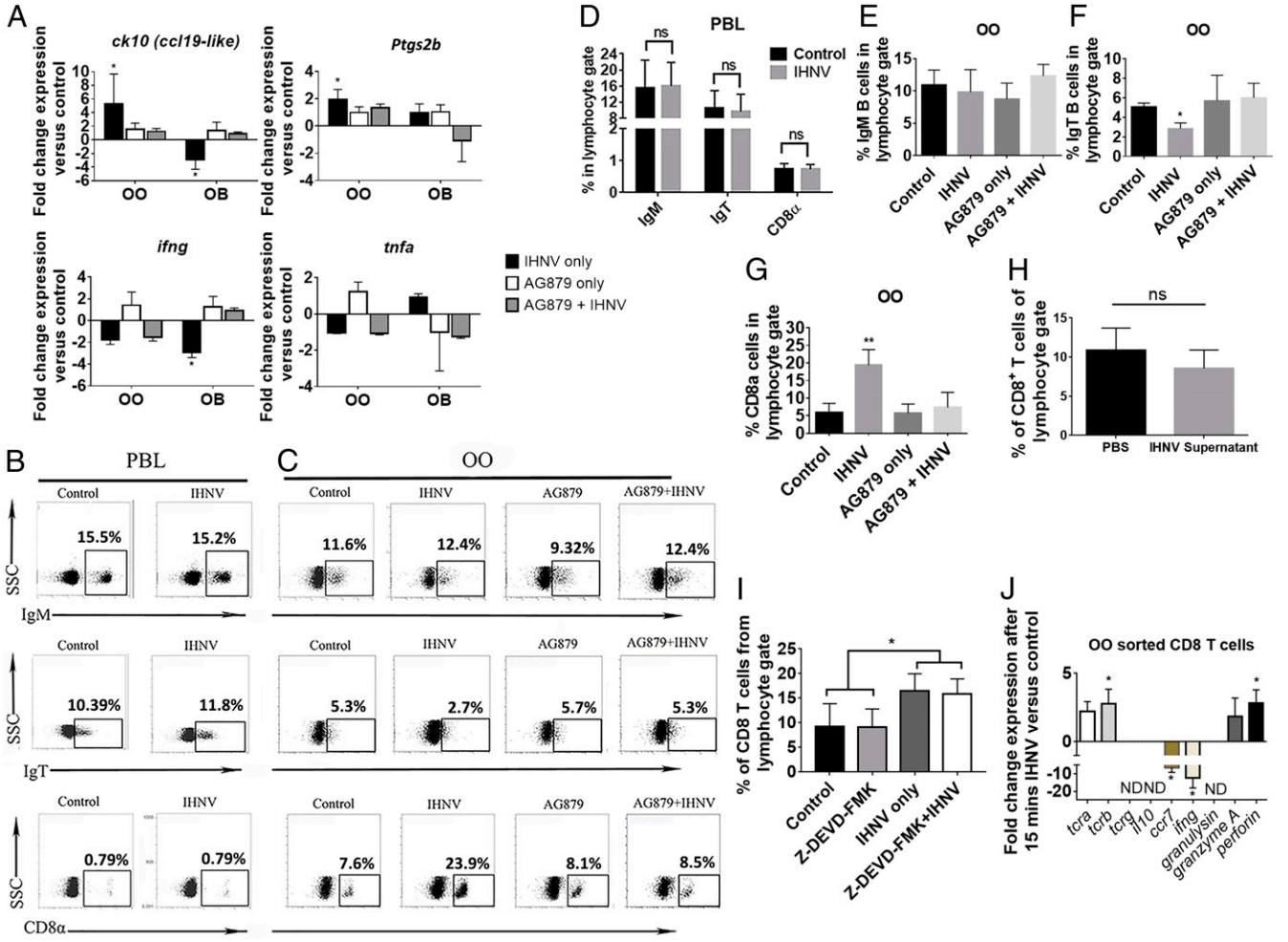

Fig. 4. Viral nasal delivery results in ultrarapid immune responses in the OO and OB of rainbow trout in a TrkA-dependent manner. (*A*) Gene expression levels of *ck10*, *ptgs2b*, *ifng*, and *tnfa* in OO and OB of control, IHNV-treated, AG879-treated, and AG879 + IHNV-treated trout. Results were analyzed by unpaired *t* test, $*P < 0.05$. (*B*) Representative dot plots of control and IHNV-treated trout PBLs and (*C*) of control and IHNV, AG879, and AG879 + IHNV trout OO showing the mean percentage of IgT^+, IgM^+, and $CD8\alpha^+$ cells from the lymphocyte gate. (*D*) Quantification of data in *B*. ns, not significant. (*E–G*) Quantification of data in *C*. Results (*A–G*) are representative of three different experiments ($n = 5$). One-way ANOVA and Tukey post hoc test, $*P < 0.05$, $**P < 0.01$. ns, not significant. (*H*) Virus-free supernatant did not induce $CD8\alpha^+$ T cell infiltration to the trout OO 15 min after IN delivery. (*I*) Quantification of $CD8\alpha^+$ T cells after nasal IHNV delivery with or without Z-DEV-FMK or vehicle. Results are representative of two independent experiments ($n = 5$). ns, not significant. $*P < 0.05$. (*J*) Gene expression levels of the *tcra, tcrb, tcrg, ccr7, ifng, granulysin, il10, granzyme A*, and *perforin* of sorted $CD8\alpha^+$ T cells from the OO of control and IHNV-treated trout. Gene expression levels in *A* and *J* were measured by RT-qPCR and normalized to the housekeeping gene *Ef1a*. ND, nondetectable. Results are representative of three different experiments ($n = 5$). Results were analyzed by unpaired *t* test, $*P < 0.05$.

remained unchanged in peripheral blood leukocytes (PBLs) of viral-treated, compared with control fish (Fig. 4 *B* and *D*). $CD8\alpha^+$ T cells increased from 7% in controls to 24% in IHNV-treated fish in the OO. Delivery of virus-free vaccine supernatant as confirmed by RT-qPCR (*SI Appendix*, Fig. S4*E*) did not trigger any CD8 responses (Fig. 4*H*). Additionally, whereas no significant changes in IgM^+ B cells were observed, we recorded a decrease in the percentage of IgT^+ B cells after nasal viral exposure (Fig. 4 *C*, *E*, and *F*). Blocking TrkA (Fig. 1*L*) abolished both the decrease in the percentage of IgT^+ B cells and the increase in $CD8\alpha^+$ T cells (Fig. 4 *C* and *G* and *SI Appendix*, Fig. S2 *D–F*). These results indicate that crypt neurons trigger ultrarapid cellular immune responses against rhabdoviruses in a TrkA-dependent manner. Blocking caspase-3 by nasal delivery of Z-DEVD-FMK did not significantly inhibit the influx of $CD8\alpha^+$ T cells into the OO (Fig. 4*I*) but effectively blocked IHNV-induced apoptosis in the OO (*SI Appendix*, Fig. S2*B*), therefore suggesting that neuronal activation (as demonstrated in the EOG and pERK experiments) and not apoptosis is the trigger of the immediate immune responses elicited by the virus.

Phenotype of CD8α T Cell Nasal Infiltrates. Sorted $CD8\alpha^+$ T cells from the OO of IHNV-treated trout showed increased expression of *tcra*, *tcrb*, *perforin*, and *granzyme A*, compared with sorted control $CD8\alpha^+$ T cells. *Ccr7* and *ifng* expression was significantly down-regulated in $CD8\alpha^+$ T cells from the OO of IHNV-treated fish, compared with those of control fish. *Il10* and *granulysin* expression could not be detected in sorted $CD8\alpha^+$ T cells from both groups (Fig. 4*J*). *Tcrg* expression levels were not detectable or did not change between both groups (Fig. 4*J*). These results indicate that $CD8\alpha^+$ T cells that rapidly respond to nasal virus delivery are nonconventional TCR$\alpha\beta$ T cells with a cytotoxic phenotype but limited *ifng* expression.

CD8α T Cell Infiltrates Originate in the OB Microvasculature. We hypothesized that the ultrarapid infiltration of $CD8\alpha^+$ T cells into the trout OO might originate from a pool of lymphocytes present at the OB microvasculature that are recruited after neuronal signals. To test this, we collected the blood from the microvasculature surrounding the OB and observed a significant

decrease in the percentage of cells within the lymphocyte gate 15 min after nasal delivery of IHNV, as measured by flow cytometry (Fig. 5 *A* and *C*). Analyses of OB microvasculature leukocytes showed no significant changes in the percentage of IgM^+ or IgT^+ B cells but a significant decrease in the percentage of $CD8\alpha^+$ T cells, from ∼2% to ∼0.5% (Fig. 5 *B* and *D*). Total $CD8\alpha^+$ T cell as well as IgM^+ B cell numbers decreased significantly while IgT^+ B cell numbers remained unchanged (Fig. 5*E*). Intravenous (i.v.) administration of FITC-conjugated dextran indicated that these effects occur without any changes in the blood–brain barrier (BBB) integrity of IHNV-treated fish (*SI Appendix*, Fig. S4 *F*–*I*). Combined, these results indicate an ultrarapid shunting of $CD8\alpha^+$ T cells from the OB to the OO.

The Interaction Between IHNV Viral Glycoprotein (G Protein) and TrkA Is Necessary for the Onset of Nasal Antiviral Immune Responses. Since HSV-secreted G protein has been previously shown to interact with mouse TrkA (26), we hypothesized that IHNV G protein may be the ligand for TrkA in rainbow trout crypt neurons. Comparison of IHNV G protein and HSV-secreted G protein indicated a low degree of amino acid conservation (*SI Appendix*, Fig. S6*A*). Amino acid sequence analysis of vertebrate TrkA molecules, on the other hand, showed a high (>50%) conservation among mouse, human, and rainbow trout TrkA (*SI Appendix*, Fig. S7*A*), including amino acid sites known to interact with NGF (27). In vivo nasal delivery of FLAG-tagged IHNV G protein (*SI Appendix*, Fig. S6*B*) showed the colocalization of TrkA and IHNV G protein 15 min after (*SI Appendix*, Fig. S7*B*). All $TrkA^+$ cells observed were $FLAG^+$. We also observed a significant decrease in the number of $TrkA^+$ cells and a significant increase in the number of $CD8\alpha^+$ T cells 15 min after IN delivery of FLAG-tagged IHNV G protein (*SI Appendix*, Fig. S7 *C* and *D*). In vivo antibody neutralization experiments showed that blocking IHNV G protein, but not N protein, rescued the loss of TrkA reactivity in crypt neurons and abolished the infiltration of $CD8\alpha^+$ T cells into the trout OO (*SI Appendix*, Fig. S7 *E* and *F*). These experiments demonstrated that the interaction between viral G protein and the crypt neuron TrkA receptor is necessary and sufficient to elicit OO immune responses.

Crypt Neurons Are Involved in Survival from Rhabdoviral Infection. Our results thus far provided evidence for the role of crypt neurons in the immune cross-talk between the OO and the CNS. Next, we asked whether viral detection by crypt neurons is necessary for survival against rhabdoviral infection, using a zebrafish

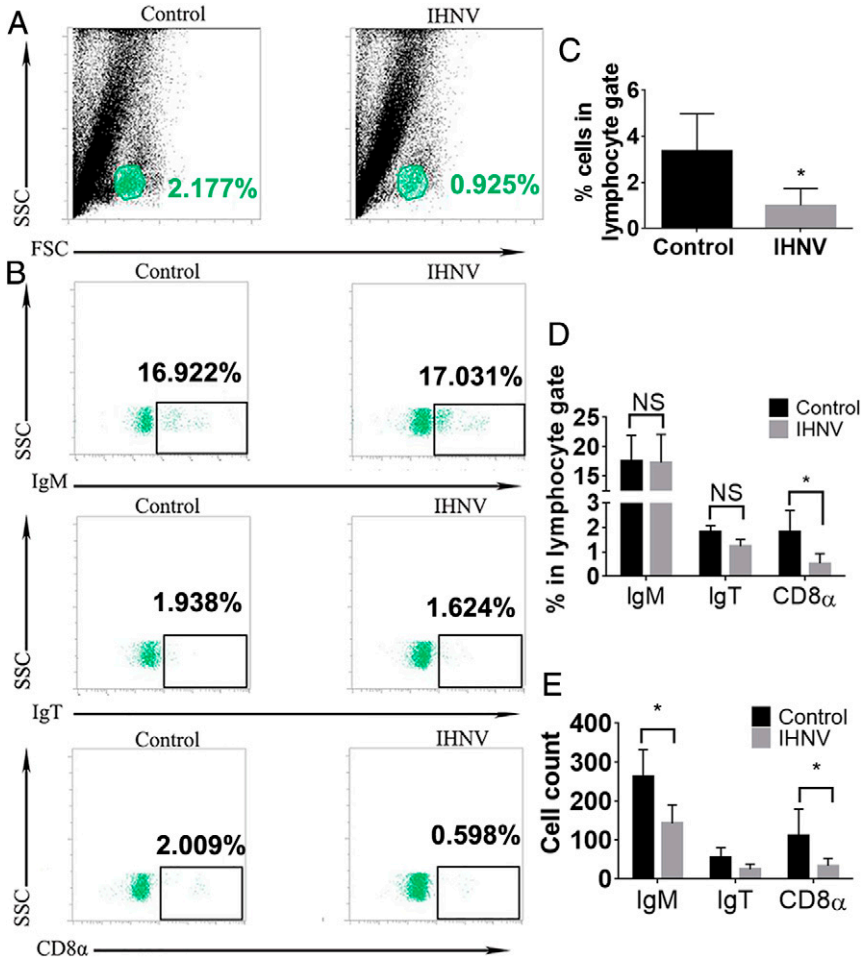

Fig. 5. $CD8\alpha^+$ T cells infiltrating the trout OO originate from the OB microvasculature, but not from peripheral blood. (*A*) Representative dot plots of control and IHNV-treated trout of cells obtained from the OB microvasculature, showing the percentage of cells within the lymphocyte gate in each group. (*B*) Representative dot plots of cells obtained from the OB microvasculature of control and IHNV-treated rainbow trout stained with mouse anti-trout IgM, mouse anti-trout IgT, and rat anti-trout CD8α, showing the mean percentage of positive cells within the lymphocyte gate. (*C*) Quantification of flow cytometry data presented in *A*. (*D*) Quantification of flow cytometry data shown in *B*. (*E*) Total cell counts for IgM^+, IgT^+, and $CD8\alpha^+$ lymphocytes in the OB microvasculature 15 min after nasal IHNV delivery. Results are representative of three different experiments ($n = 5$). Results were analyzed by unpaired *t* test, $^*P < 0.05$. NS, not significant.

(*Danio rerio*) model (Fig. 6*A*). To that end, we generated a transgenic zebrafish line which expressed the Gal4.VP16 transactivator under the *ora4* promoter and green fluorescence protein under a heart-specific promoter *cmlc2* (Fig. 6*B*). Crossing of this line with a line which expresses bacterial nitroreductase fused to mCherry revealed the presence of *ora4*+ crypt neurons from 2 dpf onward (Fig. 6 *A* and *B*). Addition of the prodrug metronidazole (Mtz) resulted in 100% ablation of crypt neurons, that started to regenerate 5 d later (7 dpf) (Fig. 6*B*). Infection of ora4^{+} ablated zebrafish with spring viremia of carp virus (SVCV) resulted in defects in *ccl19-like* chemokine expression patterns in response to infection, compared with nonablated controls (Fig. 6*C*), as measured by RT-qPCR. Crypt neuron ablation resulted in no significant differences in SVCV viral loads 15 min after exposure but increased SVCV loads 2 d postinfection (Fig. 6*D*). Importantly, challenge with SVCV revealed that, in the absence of crypt neurons, zebrafish are more susceptible to viral infection (Fig. 6*E*). These results demonstrate that crypt neurons regulate immune responses in response to viral infection and that these responses are essential for host survival and may be involved in viral clearance.

Discussion

The complex and bidirectional interactions between the nervous system and the immune system are key for the success and survival of all animal species. Apart from homeostatic functions, neuroimmune interactions are vital for protection of neuronal tissues from invading pathogens, as well as from damaging host immune responses. For instance, *Caenorhabditis elegans* responds to microorganisms with protective behavioral avoidance responses (28, 29). This behavior depends on G protein-coupled receptors expressed by chemosensory neurons (30).

Viral pathogens have evolved different strategies to invade the CNS, including exploiting the olfactory route or crossing the BBB (15, 16). HSV-1, influenza A virus, and parainfluenza viruses are examples of viral pathogens that enter the CNS through the OO in mammals (15, 16, 31). CNS immune responses need to be quick and tightly controlled because, otherwise, they may lead to meningitis, encephalitis, meningoencephalitis, or even death (15). Our results reveal a model of viral recognition by the vertebrate peripheral nervous system in which OSNs are able to sense microbes and use electrical decoding to trigger ultrafast immune responses in bony fish.

The present study identifies a specific type of OSN, the crypt neuron, that is able to initiate rapid immune responses when the G protein of a virus, IHNV, binds TrkA. We envisage three features of crypt neurons that make them ideal for pathogen detection: (*i*) They are strategically located in the most apical

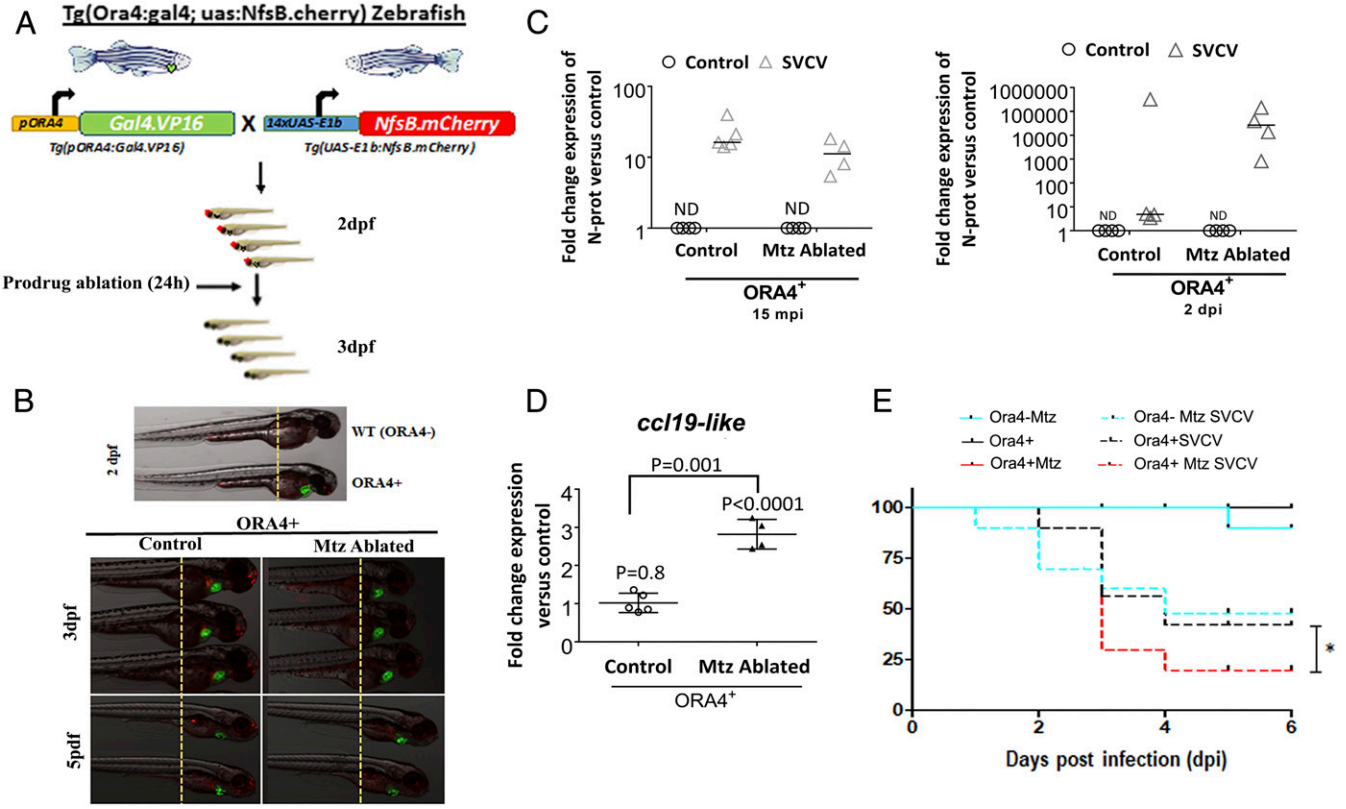

Fig. 6. Ablation of crypt neurons results in increased susceptibility to rhabdoviral infection in zebrafish. (*A* and *B*) Schematic representation of the generation of *ora4* transgenic zebrafish and ablation of crypt neurons by delivery of the prodrug metronidazole (Mtz) into the water for 24 h. (*C*) Expression of *ccl19-like* chemokine in whole zebrafish larvae 15 min after infection with SVCV, as measured by RT-qPCR. Each symbol represents a pool of 10 larvae. Results are expressed as the fold change in expression compared with uninfected controls. Expression levels were normalized to the *rps11* as housekeeping gene. Data are expressed as the mean fold change compared with the control group using the Pfaffl method. Results are representative of three different experiments ($n = 5$). Results were analyzed by unpaired *t* test. (*D*) Relative SVCV viral loads as measured by N protein expression levels 15 min and 2 d after SVCV infection in ORA4^{+} zebrafish and ORA4^{+} + Mtz (ablated) zebrafish. Each symbol represents a pool of 10 larvae. Results are expressed as mean level of N protein expression measured by RT-qPCR compared with uninfected controls. ND, nondetectable. *P* values were obtained by unpaired *t* test. (*E*) Percent survival of wild-type (ORA4^{-}) and transgenic (ORA4^{+}) zebrafish larvae that were ablated (+Mtz) or not in response to SVCV infection. Results are representative of two independent experiments ($n = 30$ per group). The asterisk indicates statistically significant differences between groups. Statistical analysis was performed by the Gehan–Breslow–Wilcoxon method ($P < 0.05$).

part of the teleost olfactory epithelium and so are the most exposed to invading microorganisms; (*ii*) they only constitute a small percentage of all cells in the OO of trout, and therefore loss of TrkA expression and cell death does not compromise large numbers of OSNs; and (*iii*), because crypt neurons are replaced within few days, the refractory period to recover pathogen sensors in the trout OO is relatively quick. The effects of a secondary pathogen encounter before crypt neuron regeneration remain to be explored, but it is possible that compensatory mechanisms are in place while crypt neurons replenish. Additionally, whether loss of crypt neurons results in defects in sensory function or behavior requires further evaluation.

We report here that instant activation of OSNs allows the olfactory system to trigger rapid immune responses. Importantly, we observed up-regulation of *ccl19-like* chemokine and *ptgs2b*, in the olfactory epithelium where the virus was delivered, but down-regulation of the same genes in other regions of the olfactory circuitry, such as the OB. These regional changes in immune gene expression may suggest cooperation between both regions of the circuit, likely to achieve cytokine gradients (like CCL19) that guide cells from one compartment to the other and control viral infection at the entry point. Changes in gene expression were accompanied by the recruitment of nonconventional CD8α$^+$ T cells within minutes. The rapid nature of these responses can be achieved thanks to cellular and molecular events that are completed within the same time frame. For instance, previous studies have shown that clearance of TrkA from the cell surface following addition of ligand takes place within minutes (32). Caspase-3 activation is also known to only take a few minutes (33). With regard to regulation of gene expression, primary response genes do not require de novo protein synthesis for their expression (34–36), and they are involved in neuronal responses, as well as stress and immune responses. Finally, the nasal epithelium has a well-developed and rich vasculature system (37), and nasal blood vessels open at very high speeds in response to chemical, mechanical, or thermal stimuli. Since odorants are known to evoke vasculature responses in the olfactory bulb of rodents (38), this type of vascular response may afford the nasal CD8$^+$ T cell infiltrates here reported. Further studies will address this hypothesis.

Infiltrating CD8α$^+$ T cells in trout OO originated in the CNS and expressed markers of cytotoxic T cells, such as *perforin* and *granzyme A*, in response to nasal viral delivery. These findings suggest that the function of these infiltrates may be killing virally infected neurons to stop progression of the infection to the OB and other CNS regions. Future functional studies will ascertain the killing capabilities of early recruited CD8α$^+$ T cells in the fish OO.

TrkA is utilized by several pathogens, including parasites such as *Trypanosoma* (14) and viruses such as HSV (26), to invade host neurons or to manipulate neuronal behavior. Interestingly, secreted HSV G protein is able to bind TrkA in mouse skin neurons and modify neuronal dendrite outgrowth (26). Additionally, HSV-2–secreted G protein is known to bind chemokines and enhance, in this manner, cell migration (39). Several fish rhabdoviruses, including IHNV, SVCV, and viral hemorrhagic septicemia virus (VSHV), are neurotropic (17, 40, 41). We provide evidence that the G protein of aquatic IHNV also interacts with TrkA$^+$ crypt neurons. These findings suggest that G proteins from different neurotropic viruses have coopted binding TrkA expressed in different neuronal types as a strategy to invade their hosts. Importantly, our work shows that the arms race between host and pathogen has resulted in efficient immune responses evoked by the TrkA–viral G protein interaction.

One of the most striking findings of the present study was the immunological cross-talk between the OO and the OB. Previous studies in mice have shown that infiltration of CCR7$^+$ CD8$^+$ T cells from the lymph nodes into the OB occurs in response to neurotropic viral infection of the OB (42). In contrast, our experiments indicate that OB responses take place very rapidly and in the absence of viral infection. The expression of *ck10*, a CCL19-like chemokine in trout (25), was quickly up-regulated in the OO and down-regulated in the OB in response to nasal viral delivery. These findings suggest that the CCL19-CCR7 CD8 T cell axis is a conserved hallmark of antiviral immune responses in neuronal tissues in both bony fish and mammals and that this axis is activated even when the virus does not penetrate into the CNS. Through a mechanism not explored in the present study, the OB turns viral-evoked electrical signals into immune responses within minutes. Future studies should address which molecules (i.e., neurotransmitters or neuropeptides) are responsible for the changes in the OB microvasculature and T cell migration following nasal viral delivery.

In conclusion, our findings demonstrate a mechanism of neuroimmune interaction by which OSNs can rapidly initiate antiviral immune responses in the OO–OB axis via a TrkA-sensing mechanism of viral G proteins. Understanding how the interaction between viral antigens and OSNs regulates innate and adaptive immune responses in the nasal mucosa and CNS can potentially help improve the efficacy and safety of nasal vaccines.

Materials and Methods

Animals, Nasal Delivery of Virus, and Tissue Sampling. All rainbow trout studies were reviewed and approved by the Institutional Animal Care and Use Committee (IACUC) at the University of New Mexico, protocol 16-200384-MC. For nasal delivery of virus studies, rainbow trout (mean weight of 50 to 150 g) received 30 μL of live attenuated infectious hematopoietic necrosis virus (IHNV) vaccine (2×10^8 PFU/mL) or phosphate-buffered saline (PBS) in each naris. Additional controls ($n = 4$) included trout that received intranasally virus-free vaccine supernatant or fresh DMEM never exposed to virus or infected cells. Live attenuated IHNV stocks were prepared from IHNV strain 220-90 in epithelioma papulosum cyprini (EPC) cells as explained in ref. 17. Rainbow trout ($n = 4$) received 30 μL of PBS containing 50 μg of poly (I:C) (Sigma) in each naris and were collected 4 h later as a positive control for caspase-3 apoptosis (43) in vivo. For the TrkA-blocking experiment, rainbow trout ($n = 20$) received 30 μL of 10 μM AG879 or vehicle 30 min before viral delivery, as described in Fig. 1*L*. The olfactory organ (OO) and olfactory bulb (OB) were snap frozen, and cryoblocks were used for immunostaining or kept in RNAlater (ThermoFisher) for gene expression studies.

Zebrafish (*Danio rerio*) were obtained from the Zebrafish International Resource Center and mated, staged, raised, and processed as described (44). The line *Tg(UAS-E1b:nfsb-mCherry)*^{c264} has been previously reported (45). The experiments performed comply with the Guidelines of the European Union Council (Directive 2010/63/EU) and the Spanish RD 53/2013. Experiments and procedures were performed as approved by the Bioethical Committees of the University of Murcia (approvals 537/2011, 75/2014, and 216/2014).

Details about the experimental approaches for electrophysiology recordings, microscopy, Western blotting, recombinant protein production, gene expression analysis, generation of transgenic zebrafish lines, and statistical analyses can be found in *SI Appendix, SI Methods*.

ACKNOWLEDGMENTS. We thank Hossein Goudarzi for help with graphics; I. Fuentes and P. Martínez for excellent technical assistance; Dr. Pilar Fernández-Somalo for the SVCV strain; Dr. Fumio Takizawa for the CD8 antibody; Profs. D. Halpern and M. Parsons for the Tg(UAS-E1b:nfsb-mCherry)^{c264}; and Dr. Weiming Li for help with the preliminary data in the electrophysiology assays. This work was supported by US Department of Agriculture and Food Research Initiative Grant 2DN70-2RDN7 (to I.S.), NSF Integrative Organismal Systems (IOS) Award 1755348 (to I.S. and M.H.), and NIH Centers of Biomedical Research Excellence Grant P20GM103452, as well as Spanish Ministry of Economy and Competitiveness Grants BIO2014-52655-R and BIO2017-84702-R (to V.M.), and cofunded with Fondos Europeos de Desarrollo Regional/European Regional Development Funds. C.K. was funded by the Stephanie Ruby Fellowship and NSF IOS Award 1456940 (to I.S.).

1. D. Arendt, The evolution of cell types in animals: Emerging principles from molecular studies. *Nat. Rev. Genet.* **9**, 868–882 (2008).
2. I. M. Chiu *et al*., Bacteria activate sensory neurons that modulate pain and inflammation. *Nature* **501**, 52–57 (2013).
3. F. A. Pinho-Ribeiro, W. A. Verri, Jr, I. M. Chiu, Nociceptor sensory neuron–Immune interactions in pain and inflammation. *Trends Immunol.* **38**, 5–19 (2017).
4. J. Sun, Y. Liu, A. Aballay, Organismal regulation of XBP-1-mediated unfolded protein response during development and immune activation. *EMBO Rep.* **13**, 855–860 (2012).
5. A. Sepahi, I. Salinas, The evolution of nasal immune systems in vertebrates. *Mol. Immunol.* **69**, 131–138 (2016).
6. L. Tacchi *et al*., Nasal immunity is an ancient arm of the mucosal immune system of vertebrates. *Nat. Commun.* **5**, 5205 (2014).
7. D. Biechl, K. Tietje, G. Gerlach, M. F. Wullimann, Crypt cells are involved in kin recognition in larval zebrafish. *Sci. Rep.* **6**, 24590 (2016).
8. G. Ahuja *et al*., Zebrafish crypt neurons project to a single, identified mediodorsal glomerulus. *Sci. Rep.* **3**, 2063 (2013).
9. S. Catania *et al*., The crypt neurons in the olfactory epithelium of the adult zebrafish express TrkA-like immunoreactivity. *Neurosci. Lett.* **350**, 5–8 (2003).
10. A. Germanà *et al*., S100 protein-like immunoreactivity in the crypt olfactory neurons of the adult zebrafish. *Neurosci. Lett.* **371**, 196–198 (2004).
11. M. L. Grimes *et al*., Endocytosis of activated TrkA: Evidence that nerve growth factor induces formation of signaling endosomes. *J. Neurosci.* **16**, 7950–7964 (1996).
12. E. Cattaneo, R. McKay, Proliferation and differentiation of neuronal stem cells regulated by nerve growth factor. *Nature* **347**, 762–765 (1990).
13. M. V. Sofroniew, C. L. Howe, W. C. Mobley, Nerve growth factor signaling, neuroprotection, and neural repair. *Annu. Rev. Neurosci.* **24**, 1217–1281 (2001).
14. M. de Melo-Jorge, M. PereiraPerrin, The Chagas' disease parasite Trypanosoma cruzi exploits nerve growth factor receptor TrkA to infect mammalian hosts. *Cell Host Microbe* **1**, 251–261 (2007).
15. O. O. Koyuncu, I. B. Hogue, L. W. Enquist, Virus infections in the nervous system. *Cell Host Microbe* **13**, 379–393 (2013).
16. I. Mori, Y. Nishiyama, T. Yokochi, Y. Kimura, Olfactory transmission of neurotropic viruses. *J. Neurovirol.* **11**, 129–137 (2005).
17. S. E. LaPatra *et al*., Characterization of IHNV isolates associated with neurotropism. *Vet. Res.* **26**, 433–437 (1995).
18. T. E. Allsopp, M. F. Scallan, A. Williams, J. K. Fazakerley, Virus infection induces neuronal apoptosis: A comparison with trophic factor withdrawal. *Cell Death Differ.* **5**, 50–59 (1998).
19. T. T. Chou, J. Q. Trojanowski, V. M.-Y. Lee, A novel apoptotic pathway induced by nerve growth factor-mediated TrkA activation in medulloblastoma. *J. Biol. Chem.* **275**, 565–570 (2000).
20. J.-F. Lavoie *et al*., TrkA induces apoptosis of neuroblastoma cells and does so via a p53-dependent mechanism. *J. Biol. Chem.* **280**, 29199–29207 (2005).
21. W. Gomes-Leal *et al*., Neurotropism and neuropathological effects of selected rhabdoviruses on intranasally-infected newborn mice. *Acta Trop.* **97**, 126–139 (2006).
22. V. Nikoletopoulou *et al*., Neurotrophin receptors TrkA and TrkC cause neuronal death whereas TrkB does not. *Nature* **467**, 59–63 (2010).
23. B. Y. Lau, P. Mathur, G. G. Gould, S. Guo, Identification of a brain center whose activity discriminates a choice behavior in zebrafish. *Proc. Natl. Acad. Sci. U.S.A.* **108**, 2581–2586 (2011).
24. M. Dieris, G. Ahuja, V. Krishna, S. I. Korsching, A single identified glomerulus in the zebrafish olfactory bulb carries the high-affinity response to death-associated odor cadaverine. *Sci. Rep.* **7**, 40892 (2017).
25. A. Sepahi *et al*., CK12a, a CCL19-like chemokine that orchestrates both nasal and systemic antiviral immune responses in Rainbow trout. *J. Immunol.* **199**, 3900–3913 (2017).
26. J. R. Cabrera *et al*., Secreted herpes simplex virus-2 glycoprotein G modifies NGF-TrkA signaling to attract free nerve endings to the site of infection. *PLoS Pathog.* **11**, e1004571 (2015).
27. C. Wiesmann, M. H. Ultsch, S. H. Bass, A. M. de Vos, Crystal structure of nerve growth factor in complex with the ligand-binding domain of the TrkA receptor. *Nature* **401**, 184–188 (1999).
28. C. I. Bargmann, J. H. Thomas, H. R. Horvitz, Chemosensory cell function in the behavior and development of Caenorhabditis elegans. *Cold Spring Harb. Symp. Quant. Biol.* **55**, 529–538 (1990).
29. Y. Zhang, H. Lu, C. I. Bargmann, Pathogenic bacteria induce aversive olfactory learning in Caenorhabditis elegans. *Nature* **438**, 179–184 (2005).
30. R. McMullan, A. Anderson, S. Nurrish, Behavioral and immune responses to infection require Gαq- RhoA signaling in C. elegans. *PLoS Pathog.* **8**, e1002530 (2012).
31. C. N. Detje *et al*., Local type I IFN receptor signaling protects against virus spread within the central nervous system. *J. Immunol.* **182**, 2297–2304 (2009).
32. F. Lebrun-Julien, B. Morquette, A. Douillette, H. U. Saragovi, A. Di Polo, Inhibition of p75(NTR) in glia potentiates TrkA-mediated survival of injured retinal ganglion cells. *Mol. Cell. Neurosci.* **40**, 410–420 (2009).
33. L. Tyas, V. A. Brophy, A. Pope, A. J. Rivett, J. M. Tavaré, Rapid caspase-3 activation during apoptosis revealed using fluorescence-resonance energy transfer. *EMBO Rep.* **1**, 266–270 (2000).
34. S. Bahrami, F. Drabløs, Gene regulation in the immediate-early response process. *Adv. Biol. Regul.* **62**, 37–49 (2016).
35. B. H. Cochran, A. C. Reffel, C. D. Stiles, Molecular cloning of gene sequences regulated by platelet-derived growth factor. *Cell* **33**, 939–947 (1983).
36. T. Fowler, R. Sen, A. L. Roy, Regulation of primary response genes. *Mol. Cell* **44**, 348–360 (2011).
37. S. Gizurarson, Anatomical and histological factors affecting intranasal drug and vaccine delivery. *Curr. Drug Deliv.* **9**, 566–582 (2012).
38. E. Chaigneau, M. Oheim, E. Audinat, S. Charpak, Two-photon imaging of capillary blood flow in olfactory bulb glomeruli. *Proc. Natl. Acad. Sci. U.S.A.* **100**, 13081–13086 (2003).
39. N. Martínez-Martín, A. Viejo-Borbolla, A. Alcami, Herpes simplex virus particles interact with chemokines and enhance cell migration. *J. Gen. Virol.* **97**, 3007–3016 (2016).
40. T. Ito, J. Kurita, K. Mori, N. J. Olesen, Virulence of viral haemorrhagic septicaemia virus (VHSV) genotype III in rainbow trout. *Vet. Res. (Faisalabad)* **47**, 4 (2016).
41. Y. Wang *et al*., Comparative transcriptome analysis of zebrafish (Danio rerio) brain and spleen infected with spring viremia of carp virus (SVCV). *Fish Shellfish Immunol.* **69**, 35–45 (2017).
42. J. Cupovic *et al*., Central nervous system stromal cells control local CD8+ T cell responses during virus-induced neuroinflammation. *Immunity* **44**, 622–633 (2016).
43. K. Kanaya *et al*., Innate immune responses and neuroepithelial degeneration and regeneration in the mouse olfactory mucosa induced by intranasal administration of Poly(I:C). *Cell Tissue Res.* **357**, 279–299 (2014).
44. M. Westerfield, *The Zebrafish Book. A Guide for the Laboratory Use of Zebrafish Danio (Brachydanio) Rerio* (University of Oregon Press, Eugene, OR, 2000).
45. J. M. Davison *et al*., Transactivation from Gal4-VP16 transgenic insertions for tissue-specific cell labeling and ablation in zebrafish. *Dev. Biol.* **304**, 811–824 (2007).